Steady, supercritical flow in collapsible tubes. Part 2. Theoretical studies

By MICHAEL E. McCLURKEN, IFIYENIA KECECIOGLU, ROGER D. KAMM AND ASCHER H. SHAPIRO

Fluid Mechanics Laboratory, Department of Mechanical Engineering, Massachusetts Institute of Technology, Cambridge, Massachusetts 02139, U.S.A.

Theories are developed to explain the experimental observations of steady, supercritical flow in compliant, partially collapsed tubes, presented in the companion paper (part 1).

It is shown that the measured curves of area *vs.* distance are governed by a combination of (i) friction and gravity, which produce mean gradients of area, and (ii) longitudinal bending and tension forces, which produce standing waves of area superposed upon the mean gradients. The experiments confirm the one-dimensional theory for the mean gradients: (i) in the absence of gravity, friction causes a pressure rise and a positive mean gradient of area; (ii) a downward slope can cancel gravity and lead asymptotically to a uniform state having zero gradients of pressure and area.

The inviscid dispersion relationship for area waves due to longitudinal bending and tension is developed, based on a simple, approximate model for the mechanics of the tube. The phase velocity increases as the wavelength decreases, hence the group velocity exceeds the phase velocity. Consequently, in steady flows that are supercritical with respect to the infinite-wavelength phase velocity, energy can propagate upstream and standing waves of area may appear.

In the experiments of part 1, longitudinal tension predominated over longitudinal bending. The measured wavelengths of standing waves were found to be in general agreement with the dispersion relationship for tension-induced area waves. The observed streamwise growth of standing area waves is interpreted physically as the attenuation of waves radiating upstream from a source of disturbance such as a shock-like rapid increase of area. The rate of wave attenuation indicates that the skin-friction coefficient has a large out-of-phase oscillatory component. The observed steepness of shock transitions agrees with an approximate theory based on treating the forward portion of the shock as the rearward part of the standing wave train that the shock drives upstream.

1. Introduction

This is a companion paper to Kececioglu *et al.* (1981), hereinafter referred to as part 1. In part 1, experimental studies were described for steady, initially supercritical flow in compliant, partially collapsed tubes. In the present paper, the experimental results are explained within a theoretical framework, and quantitative comparisons are made between theory and experiments.

2. Formulation of the theoretical model

2.1. *Strategy*

Flows of the type discussed in part 1 are, for several reasons, complex in detail: (i) the three-dimensionality of the tube configuration affects both the fluid mechanics and the structural mechanics; (ii) the mechanics of the flow and of the structure are coupled; and (iii) strong nonlinearities are present. Having in mind that rigorous theoretical solutions, even if attainable, might well obscure the most important physical phenomena, we seek here a relatively simple, albeit approximate, theoretical model which can provide simple insights into the dominant physical features of the problem.

Except in the rapid area expansion of a shock wave, the flow may reasonably be treated as one-dimensional. The greatest obstacle then to a simple theory is the complex structural mechanics of the partially collapsed tube, particularly when longitudinal tension and longitudinal bending play significant roles.

Although the paper is directed mainly to steady flows, time-dependent terms are included in the fluid equations in order that wave propagation, which proves to be fundamental to the understanding even of a steady flow, may be studied.

2.2. *The flow model*

The flow is treated as one-dimensional in terms of the pressure, $p(x,t)$, and the velocity, $u(x,t)$, which are both assumed to be uniform over each cross-section of the tube.

The pressure is nearly uniform if the longitudinal area gradient $(1/\alpha)(d\alpha/d\xi)$ is sufficiently small, or, equivalently, if the characteristic wavelength of area change is large compared with the local tube diameter.

The flows of part 1 are typically turbulent. Except in a shock transition, therefore, velocity profiles are approximately consistent with the one-dimensional assumption. In shock transitions, particularly if boundary-layer separation occurs, the assumed uniformity of u might entail serious error.

Viscous effects are represented by the skin-friction coefficient, $f \equiv 2\tau_w/\rho u^2$, where τ_w is the wall shear stress, and ρ the fluid density. We assume subsequently that f has two components. The first part, $\bar{f}$, is constant and equal to the value appropriate for steady, fully developed turbulent flow in a tube of uniform cross-sectional area. The second part, f', represents a small perturbation from $\bar{f}$, the physical basis of which is discussed later in connection with the growth of standing waves.

(a) *Continuity equation.* For a time-varying, incompressible, one-dimensional flow in a compliant tube of variable area $A(x,t)$, conservation of mass is expressed by

$$\frac{\partial A}{\partial t} + \frac{\partial}{\partial x}(uA) = 0. \tag{1}$$

(b) *Momentum equation.* For an unsteady, sloping flow with skin friction τ_w, the equation of motion is

$$\frac{\partial u}{\partial t} + u\frac{\partial u}{\partial x} + \frac{1}{\rho}\frac{\partial p}{\partial x} + g\frac{dz}{dx} + 2\frac{fu^2}{D_e} = 0, \tag{2}$$

where D_e is the hydraulic diameter, g the acceleration of gravity, and z the local elevation in the g-field.

2.3. *The tube model*

In the absence of longitudinal tension and bending forces, the local tube law $\mathscr{P}(\alpha)$ suffices to connect the local area with the local transmural pressure. The function $\mathscr{P}(\alpha)$ may be determined either theoretically (Flaherty, Keller & Rubinow 1972) or experimentally (e.g., part 1 figure 7).

Our task now – a difficult one – is to develop an appropriately simple area relationship when tension and bending forces are significant.

Considered as an elastic structure, the compliant tube is a three-dimensional, thin-walled shell of complex shape. For application to a one-dimensional flow model, however, all that we require is a reasonable approximation to the way in which the local area ratio α depends upon the x-derivatives of α, upon the elastic properties of the wall, and upon the transmural pressure and longitudinal tension. The model described below achieves the desired simplicity.

A significant complication is that the cross-sectional *shape* depends not only upon the local area ratio, $\alpha \equiv A/A_0$, but also upon longitudinal tension and bending effects. Over the range of area ratios from about 0·3 to about 0·8, however, in which most of the interesting supercritical flow patterns of part 1 occur, the cross-section resembles a flattened ellipse.

Accordingly, we assume, *solely for the purpose of estimating the effects of longitudinal tension and bending*, that the tube cross-section is of the shape shown in figure 1. Two parallel surfaces separated by the distance $2y$ are connected by semicircles of radius y. As the separation $2y$ changes, the cross-sectional area also changes. However, since the perimeter is constant and equal to that of a circle of radius $R_0 = \frac{1}{2}D_0 = (A_0/\pi)^{\frac{1}{2}}$, each straight segment is of length $\pi(R_0 - y)$. Thus the cross-sectional area may be expressed as

$$A = \pi y (D_0 - y) \tag{3}$$

or, in dimensionless terms,

$$\alpha \equiv \frac{A}{A_0} = 4\frac{y}{D_0}\left(1 - \frac{y}{D_0}\right), \quad \frac{y}{D_0} = \frac{1 - (1-\alpha)^{\frac{1}{2}}}{2}. \tag{4}$$

In applying equation (4), the values of A_0 and D_0 used were those pertaining to the longitudinal strain ϵ_x of the particular experiment.

2.4. *Modification of the local tube law for longitudinal tension and bending*

(a) *The additive postulate.* The local tube law, $\mathscr{P}(\alpha)$, is governed by a single stiffness, that due to circumferential bending. However, when the cross-sectional area varies longitudinally, longitudinal bending stiffness and membrane stiffness due to longitudinal tension are also capable of resisting changes of shape and area.

For our simple quasi-one-dimensional model of the tube mechanics, we postulate that the three stiffnesses above are separable and act additively to support the transmural pressure. Thus the modified tube law is written as

$$p - p_e = K_p \mathscr{P}(\alpha) + \Delta P_t + \Delta P_b. \tag{5}$$

Here ΔP_t and ΔP_b represent the stiffness of the tube against collapse due to the effects of axial tension and bending, respectively.

(b) *Circumferential bending.* In the geometry of figure 1, the circumferential bending
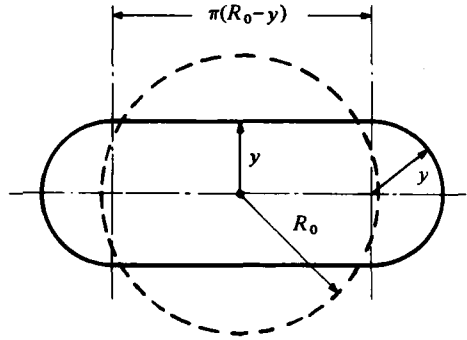
FIGURE 1. Geometric model used to estimate stiffnesses due to longitudinal tension and bending.

stiffness would be physically due to the forces required to bend the semicircular end regions to a new radius of curvature. However, in applying equation (5), we make the assumption that the circumferential stiffness function $\mathscr{P}(\alpha)$ is the same as that determined for the *actual* tube under *longitudinally uniform* conditions.

(c) *Axial tension.* To formulate an estimate of the tension stiffness ΔP_t, consider in figure 1 the transverse displacements of the straight segments of the wall. If the longitudinal radius of curvature in an axial plane is R, longitudinal membrane forces are capable of supporting a pressure difference of magnitude

$$\Delta P_t = -\frac{T}{R} \simeq -\frac{T \partial^2 y}{\partial x^2} = -\left(\frac{T}{D_0}\right)\frac{\partial^2(y/D_0)}{\partial \xi^2}, \tag{6}$$

where $T = \epsilon_x E h$ is the axial force per unit perimeter resulting from the axial strain ϵ_x, h is the wall thickness, and E is the modulus of elasticity. It has been assumed for (6) that the slope $\partial y/\partial x$ is small; or, more precisely, that $(\partial y/\partial x)^2 \sim (\Delta y/\lambda)^2 \ll 1$, where λ is the characteristic distance over which the variation Δy occurs.

Expressing $\partial^2 y/\partial x^2$ in terms of α-derivatives by means of (4), we get

$$\Delta P_t = -\frac{T/D_0}{4}\left[\frac{1}{(1-\alpha)^{\frac{1}{2}}}\frac{\partial^2 \alpha}{\partial \xi^2} + \frac{1}{2(1-\alpha)^{\frac{3}{2}}}\left(\frac{\partial \alpha}{\partial \xi}\right)^2\right]. \tag{7}$$

Here, the ratio of the second to the first term within the square brackets is of order $\Delta\alpha/2(1-\alpha)$, where $\Delta\alpha$ is the change in α that occurs over the characteristic distance λ. For typical standing waves of area (part 1), $\Delta\alpha \simeq 0.05$ and $\alpha \simeq 0.4$, for which values the ratio of the nonlinear term to the linear term is only of order 0.04. In what follows, therefore, we neglect the second term of (7) and retain only the linear term. We note, however, that, in shock waves, $\Delta\alpha \simeq 0.6$ and $\alpha \simeq 0.7$; the two terms are then of the same order.

Equation (7) now simplifies to

$$\Delta P_t \simeq -\frac{T/D_0}{4(1-\alpha)^{\frac{1}{2}}}\frac{\partial^2 \alpha}{\partial \xi^2}. \tag{8}$$

Both this and equation (7) blow up when $\alpha \to 1$, not altogether surprisingly. A more detailed consideration of the tube mechanics shows that the treatment employed here, namely the combination of the geometry of figure 1 with (5) and (6), becomes quite unrealistic when the tube is nearly round; for instance, (3) yields $(dy/dx)/(dA/dx) \to \infty$ as $\alpha \to 1$. Accordingly, it is improper to use the approximation of (8) for α too close to

unity. For this reason, together with that given in the preceding paragraph, it is improper to use (8) for the rearward part of a shock wave.

Strictly speaking, T is a function of axial distance because of skin friction forces. However, the variation of T was generally small for the experiments of part 1. No significant features of behaviour are lost by the further assumption that T is constant.

(*d*) *Longitudinal bending.* The stiffness against bending of the two parallel surfaces of figure 1 is given by

$$\Delta P_b = EI \frac{\partial^4 y}{\partial x^4} = \frac{EI}{D_0^3} \frac{\partial^4 (y/D_0)}{\partial \xi^4},\qquad(9)$$

where the moment of inertia I is equal to $h^3/[12(1-\nu^2)]$, and ν is Poisson's ratio.

As in the case of the simplification leading to (8), only the linear term is retained when y is expressed in terms of α through (4). The resulting approximate expression is

$$\Delta P_b \simeq \frac{K_p}{32(1-\alpha)^{\frac{1}{2}}} \frac{\partial^4 \alpha}{\partial \xi^4}.\qquad(10)$$

The four nonlinear terms neglected are in fact small compared with the surviving linear term of (10), except in shock waves. And, as with the tension term, the model leading to (10) loses validity as $\alpha \to 1$.

(*e*) *The modified tube law.* Combination of (5) with (8) and (10) results in

$$\frac{p-p_e}{K_p} = \mathscr{P}(\alpha) + \frac{1}{32(1-\alpha)^{\frac{1}{2}}} \frac{\partial^4 \alpha}{\partial \xi^4} - \frac{T/K_p D_0}{4(1-\alpha)^{\frac{1}{2}}} \frac{\partial^2 \alpha}{\partial \xi^2}.\qquad(11)$$

Equations (1), (2) and (11) comprise the set of governing equations for the dependent variables A, u and p in terms of the independent variables x and t. Upon differentiation of (11) to obtain $\partial p/\partial x$, and substitution of the latter into (2), we are left with two equations for A and u. Equation (2) then contains a fifth-order term, representing longitudinal bending, and a third-order term, representing longitudinal tension.

(*f*) *Evaluation of the structural model.* There is obvious crudity in several of the approximations underlying (11). Some evaluative comments follow.

(i) The assumed geometry of figure 1 is in keeping with the spirit of a one-dimensional flow model. It is used here only to estimate the stiffnesses ΔP_t and ΔP_b, whereas the circumferential bending stiffness function $\mathscr{P}(\alpha)$ is related to the actual geometry (although see comment immediately below).

(ii) The assumption that circumferential bending and longitudinal tension and bending act independently, and are thus additively superposable, is clearly incorrect for large deformations with compound curvature (e.g. a corrugated sheet is stiffer in bending than a flat sheet). Because of tube collapse, the circumferential curvature is normally very much larger than the longitudinal curvature. The effect of compound curvature is to increase the effective bending stiffness constant, K_p. This may be quite pronounced with respect to stiffness in longitudinal bending. Considering the two correction terms of (5), the formulation for ΔP_b as given by (10) is therefore of much weaker validity than the formulation of ΔP_t as given by (8).

(iii) One aspect of the coupling between the different stiffnesses is that, due to longitudinal tension, the *effective* transmural loading on the wall is variable around the perimeter, whereas the experimental function $\mathscr{P}(\alpha)$ is necessarily measured with uniform transmural loading. The non-uniform loading produced by longitudinal tension

in fact changes the shape of the cross-section and thus indirectly affects the function $\mathscr{P}(\alpha)$.

(iv) Perhaps the most difficult assumption to justify is that longitudinal bending and tension stresses, as modelled on the straight upper and lower surfaces, are representative of those acting on the entire perimeter. In our experiments, axial tension generally dominated over axial bending forces, so we neglect the latter for the present. Consider a local area minimum: $\partial^2\alpha/\partial\xi^2$ in (11) is positive, hence tension acts like a decrease in external pressure and tends to pull the upper and lower walls of figure 1 further apart, thereby increasing the area. Over much of the side walls, however, tension pulls the surfaces inward, seeming to counteract the anticipated area increase. There is no contradiction, however, since both displacements are consistent with an increase in area for a tube of fixed perimeter, i.e. both forces tend to produce a more rounded shape. Thus the net effect of tension on the entire perimeter is, with regard to cross-sectional area, at least consistent with the direction of change given by the model. But we re-iterate, as explained earlier, that the quantitative relationship that connects the longitudinal curvature with the area derivatives becomes incorrect as $\alpha \to 1$.

(v) Further complications arise when modelling unsteady flows. To account for unsteadiness in the tube law would require, in addition to those already included, terms representing wall acceleration and viscoelasticity. We make no attempt to include these.

Notwithstanding all that is said above, equation (11) appears to represent the essential tube mechanics sufficiently well for a qualitatively correct determination of those physical events that are due to longitudinal tension and bending, particularly for small-amplitude, long-wavelength phenomena. We offer two reasons for this claim, as follows: Firstly, there is the good agreement between the experimental results of part 1 with theoretical predictions based on (11). Secondly, in a related investigation in our laboratory (Swidler 1980) the theoretical calculation of tube shape of Flaherty *et al.* (1972) was modified to take account of a circumferentially varying transmural loading due to a combination of uniform transmural pressure with longitudinal tension and non-uniform longitudinal curvature. Numerical integrations of the tube contour, leading to a fairly accurate determination of the actual tube shape and cross-sectional area, provided a means for testing the validity of (8). Swidler found that, in the range $0.30 < \alpha < 0.80$, (8) is essentially correct in form, at least for small area changes. As to magnitude, the right-hand side of (8) should, according to Swidler, be decreased by a correction factor between 0.75 and 0.90; the value of the factor is only weakly dependent upon α. On the basis of Swidler's findings, (8) is expected to provide reasonably good agreement with the experimental observations in the range $0.3 < \alpha < 0.8$.

2.5. *Methods of solution*

Solutions to the governing equations were sought by two different methods.

(a) *Unsteady flow with small perturbations.* With the assumptions that A, u and f could each be expressed as the sum of a constant term plus a small-amplitude disturbance variable in both x and t, linearized analyses were performed to obtain the dispersion relationship for wave propagation and information as to wave growth and decay.

(b) *Steady flow with large perturbations.* The full nonlinear governing relationships,

equations (1), (2) and (11), were integrated numerically, with the objective of determining how the linearized results would be modified by the nonlinear terms.

3. Effects due to mean skin friction

The terms in the momentum equation that represent longitudinal bending and longitudinal tension contain the derivatives $\partial^5 \alpha / \partial \xi^5$ and $\partial^3 \alpha / \partial \xi^3$. It will be shown later that these terms are responsible mainly for wave-like variations in α that are superposed upon mean changes in α brought about by friction and gravity.

We now confine our attention to regions where these terms are negligible, and for the present we omit them from the analysis. Thus we exclude from consideration zones near attachment points to rigid tubes, and also zones of supercritical–subcritical shock transitions, for in such regions the two derivatives are generally large.

3.1. *Theory of steady flow*

We employ equation (1) with $\partial A / \partial t = 0$, equation (2) with $\partial u / \partial t = 0$, equation (5) with $p_e = $ constant and $\Delta P_t = \Delta P_b = 0$, equation (1) of part 1, and we note that $\partial / \partial \xi = d/d\xi$. Combining these, we get, as in Shapiro (1977),

$$\frac{1}{\alpha}\frac{d\alpha}{d\xi} = -\frac{1}{1-S^2}\frac{gD_0}{c_\infty^2}\frac{dz}{dx} - \frac{S^2}{1-S^2}\frac{2\bar{f}}{\alpha}, \tag{12}$$

where $\bar{f}$ is the local mean friction coefficient and $S \equiv u/c_\infty$.

(*a*) *Gravity–friction flows.* Consider a downward-sloping, supercritical flow in which the constant conditions u_∞ and α_∞ are approached asymptotically, with friction exactly counterbalanced by gravity. In equation (12), we set $d\alpha/d\xi = 0$, $\alpha = \alpha_\infty$, and the slope $dz/dx \equiv -\sin\theta$. We also define the reference velocity $u_0 \equiv Q/A_0 = u_\infty \alpha_\infty$. Thus we obtain

$$\bar{f} = \frac{gD_0}{2u_0^2}\alpha_\infty^3 \sin\theta, \tag{13}$$

from which $\bar{f}$ may be determined using the experimental data for Q, θ and α_∞ obtained in part 1.

(*b*) *Pure friction flows.* With a horizontal tube, for which $dz/dx = 0$, equation (12) yields

$$\frac{d\alpha}{d\xi} = 2\bar{f}\frac{S^2}{S^2-1}. \tag{14}$$

When $S^2 \gg 1$, this is approximated by

$$d\alpha/d\xi \simeq 2\bar{f}. \tag{15}$$

3.2. *Comparison of theoretical and experimental results*

(*a*) *Gravity–friction flows.* In figure 2, the experimental values of $\bar{f}$ inferred from the data (e.g., figures 9 and 10 of part 1) using equation (13), are compared with the accepted values for laminar and turbulent flow in smooth, circular tubes. The agreement is reasonable, considering that the values of α in the experiments were correlated with the values of Re (α ranged from 0·27 at $Re \simeq 2000$ to 0·69 at $Re \simeq 15\,000$). At the lower values of α, several factors account for the relatively large deviation from the upper
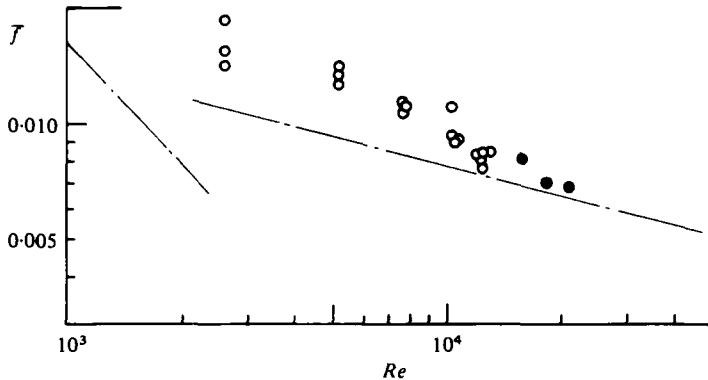
FIGURE 2. Experimental values of friction coefficient for equilibrium gravity–friction flows. Dot-dash lines show accepted values for laminar and turbulent flow in smooth circular tubes (Schlichting 1968). $\bigcirc$, $\theta = 4\cdot8°$; $\bullet$, $\theta = 9\cdot0°$.
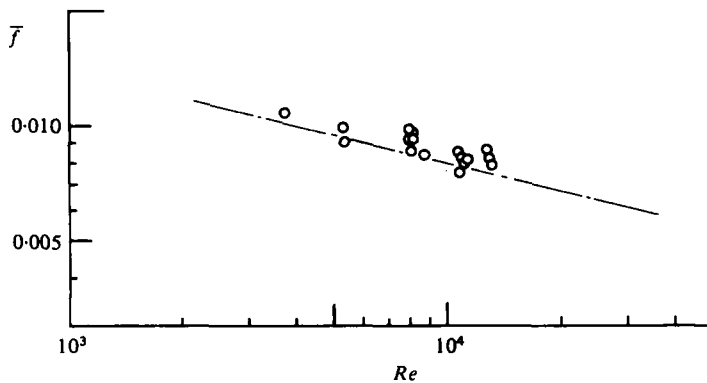
FIGURE 3. Experimental values of friction coefficient for tension–friction flows, compared with accepted curve for smooth circular tubes.

(turbulent) curve: (a) the unusual two-lobed cross-sectional configuration, with near-contact of opposite walls, (b) the relatively large frictional effect due to the catheter probe, and (c) the relatively large experimental error, since $\bar{f}$ is proportional to α_∞^3.

(b) *Pure friction flows.* Since the perimeter of the tube remains constant, the Reynolds number $Re = uD_e/\nu$ is the same at all locations, irrespective of changes of area. Thus $\bar{f}$ is anticipated to be constant provided that the flow is fully developed, at least to the degree that the friction relationship $\bar{f}(Re)$ is independent of cross-sectional shape. Most of the horizontal experiments of part 1 designated as 'tension–friction' were performed with large values of S. Thus equation (15) predicts that $d\alpha/d\xi$ = constant. Examination of the experimental results (e.g. figure 14d of part 1) shows this to be substantially correct as regards the mean variation $\alpha(\xi)$, that is, when the tension waves usually present are neglected.

The values of $\bar{f}$ inferred from the experimental data with the use of equation (15) are shown in figure 3, where they are again compared with the accepted values for smooth, circular tubes. The agreement is very satisfactory, thereby indicating that the tension waves are not large enough to affect the magnitude of the *mean* skin friction.

4. Linearized analysis

In order to investigate wave propagation, we reintroduce the terms representing longitudinal bending and tension, and then linearize the governing equations by assuming that there are only small time-dependent perturbations from a uniform state.

In terms of ξ and a dimensionless time defined as $\tau \equiv c_\infty t/D_0$, the area ratio, dimensionless speed, and friction coefficient are expressed as

$$\alpha(\xi, \tau) = \bar{\alpha} + \alpha'(\xi, \tau), \quad \alpha'/\bar{\alpha} \ll 1, \tag{16a}$$

$$S(\xi, \tau) = \bar{S} + S'(\xi, \tau), \quad S'/\bar{S} \ll 1, \tag{16b}$$

$$f(\xi, \tau) = \bar{f} + f'(\xi, \tau), \quad f'/\bar{f} \ll 1, \tag{16c}$$

where $\bar{\alpha}, \bar{S}$ and $\bar{f}$ are constants.

An unnecessary complexity is here avoided by treating c_∞ as constant. Figure 7 of part 1 shows that there is little variation of c_∞ over the range between 0·3 and 0·8. No significant physical effects are overlooked by neglecting in equations (18) and (19) the small terms in the derivative $dc_\infty/d\alpha$ which would otherwise appear.

4.1. *The perturbation equations*

The foregoing are introduced into (1) and (2) (with $\partial p/\partial x$ calculated from equation (11)). In the usual manner, only terms of first order in the primed quantities and their derivatives are retained, and higher-order terms are discarded. Thus one obtains the linearized equations:

$$\frac{\partial \alpha'}{\partial \tau} + \bar{S}\frac{\partial \alpha'}{\partial \xi} + \bar{\alpha}\frac{\partial S'}{\partial \xi} = 0, \tag{17}$$

$$\frac{\partial S'}{\partial \tau} + \bar{S}\frac{\partial S'}{\partial \xi} + \frac{1}{\bar{\alpha}}\frac{\partial \alpha'}{\partial \xi} - \frac{T/D_0}{4\rho c_\infty^2}(1-\bar{\alpha})^{-\frac{1}{2}}\frac{\partial^3 \alpha'}{\partial \xi^3} + \frac{K_p}{32\rho c_\infty^2}(1-\bar{\alpha})^{-\frac{1}{2}}\frac{\partial^5 \alpha'}{\partial \xi^5}$$
$$+ \frac{gD_0}{c_\infty^2}\frac{dz}{dx} + \frac{2\bar{S}^2\bar{f}}{\bar{\alpha}}\left(1 + 2\frac{S'}{\bar{S}} - \frac{\alpha'}{\bar{\alpha}} + \frac{f'}{\bar{f}}\right) = 0. \tag{18}$$

In order to be consistent with the small-perturbation assumptions of (16), we eliminate changes of mean area due to friction, by admitting just enough downward slope for the gravity term of equation (18) to cancel the mean friction term $2\bar{S}^2\bar{f}/\bar{\alpha}$. This is tantamount to setting equation (12) to zero.

After appropriate differentiations of equations (17) and (18), S' is eliminated, and one arrives at a sixth-order, linear partial differential equation for $\alpha'(\xi, \tau)$:

$$\frac{\partial^2 \alpha'}{\partial \tau^2} + 2\bar{S}\frac{\partial^2 \alpha'}{\partial \xi \partial \tau} + (\bar{S}^2 - 1)\frac{\partial^2 \alpha'}{\partial \xi^2} + \frac{T/D_0}{4\rho c_\infty^2}\frac{\bar{\alpha}}{(1-\bar{\alpha})^{\frac{1}{2}}}\frac{\partial^4 \alpha'}{\partial \xi^4} - \frac{K_p}{32\rho c_\infty^2}\bar{\alpha}(1-\bar{\alpha})^{-\frac{1}{2}}\frac{\partial^6 \alpha'}{\partial \xi^6}$$
$$+ 2\frac{\bar{S}^2\bar{f}}{\bar{\alpha}}\left(\frac{2}{\bar{S}}\frac{\partial \alpha'}{\partial \tau} + 3\frac{\partial \alpha'}{\partial \xi} - \frac{\bar{\alpha}}{\bar{f}}\frac{\partial f'}{\partial \xi}\right) = 0. \tag{19}$$

If variations in c_∞ were included, the term $[(\mathscr{M} - 3)/\bar{\alpha}^2](\partial \alpha'/\partial \xi)^2$ would appear on the left-hand side of (19). However, in the experiments, this term was only about 1% as large as the third term of (19).

4.2. *Wavelike solutions*

In order to investigate the wavelike behaviour inherent in flows governed by (19), we take advantage of the linearity of this equation and consider elementary wavelike solutions given by the real part of

$$
\alpha' = \hat{\alpha}\exp\left[i(\omega t - kx)\right] = \hat{\alpha}\exp\left[i\left(\frac{\omega D_0}{c_\infty}\tau - kD_0\xi\right)\right] \\
= \hat{\alpha}\exp\left[k_i D_0\xi\right]\exp\left[ik_r D_0[(c/c_\infty)\tau - \xi],\right.
\tag{20}
$$

where $\hat{\alpha}$ is a real amplitude; ω is real and equal to the circular frequency; $k = k_r + ik_i$ is the complex wavenumber; k_i is the spatial damping coefficient; $k_r = 2\pi/\lambda$ is the wavenumber; λ is the wavelength; and the phase speed c is given by

$$
c = \omega/k_r.
\tag{21}
$$

We further assume that, for reasons explained in §5, f' is sinusoidal, with the phase angle ϕ. It is represented by the real part of

$$
f' = \hat{f}\exp\left[i(\omega t - kx + \phi)\right] = \hat{f}\exp\left[i\left(\frac{\omega D_0}{c_\infty}\tau - kD_0\xi + \phi\right)\right],
\tag{22}
$$

where $\hat{f}$ is real.

Substitution of equations (20) and (22) into (19) leads to the dispersion relationship,

$$
\left[\frac{K_p}{32\rho c_\infty^2}\frac{\bar{\alpha}}{(1-\bar{\alpha})^\frac{1}{2}}\right](kD_0)^6 + \left[\frac{T/D_0}{4\rho c_\infty^2}\frac{\bar{\alpha}}{(1-\bar{\alpha})^\frac{1}{2}}\right](kD_0)^4 + \left[\frac{c_\infty^2 - (\bar{u}-c)^2}{c_\infty^2}\right](kD_0)^2 \\
+ i\frac{2\bar{S}^2\hat{f}}{\bar{\alpha}}\left[\frac{2c/c_\infty}{\bar{S}} - 3 + \frac{\hat{f}/\bar{f}}{\hat{\alpha}/\bar{\alpha}}e^{i\phi}\right](kD_0) = 0.
\tag{23}
$$

4.3. *Inviscid wave propagation*

A small amount of frictional dissipation affects mainly the decay of waves, and changes the propagation speed only slightly. We therefore examine the inviscid dispersion relationship connecting phase velocity with wavelength, found by setting $\bar{f} = 0$ in (23).

(a) *The dispersion equation.* Equation (23) now yields only real values for the wavenumber, $k_0 \equiv 2\pi/\lambda_0$, where the subscripts signify the inviscid case. By setting $\bar{u} = 0$ in (23), which is equivalent to calculating $(c - \bar{u})$, we obtain the phase velocity c *relative to the fluid*:

$$
c^2 = c_\infty^2 + \frac{\pi^2 T D_0\bar{\alpha}}{\rho\lambda_0^2(1-\bar{\alpha})^\frac{1}{2}} + \frac{\pi^4 K_p D_0^4\bar{\alpha}}{2\rho\lambda_0^2(1-\bar{\alpha})^\frac{1}{2}}.
\tag{24}
$$

Denoting the three terms on the right-hand side by c_∞^2, c_t^2 and c_b^2, one recognizes the respective effects of the three stiffnesses present, namely: (i) circumferential bending stiffness; (ii) transverse stiffness due to longitudinal membrane tension; and (iii) longitudinal bending stiffness.

For very long waves, such that $c_t \ll c_\infty$ and $c_b \ll c_\infty$, circumferential bending stiffness predominates; then $c \simeq c_\infty$ and is independent of wavelength. For very short waves, such that $c_b \gg c_\infty$ and $c_b \gg c_t$, longitudinal bending stiffness predominates; then $c \simeq c_b$, and c is proportional to λ_0^{-2}. In the intermediate ranges of wavelengths, no simple rule prevails: the relationship between c and λ_0 depends upon the ratios of the three stiffnesses.
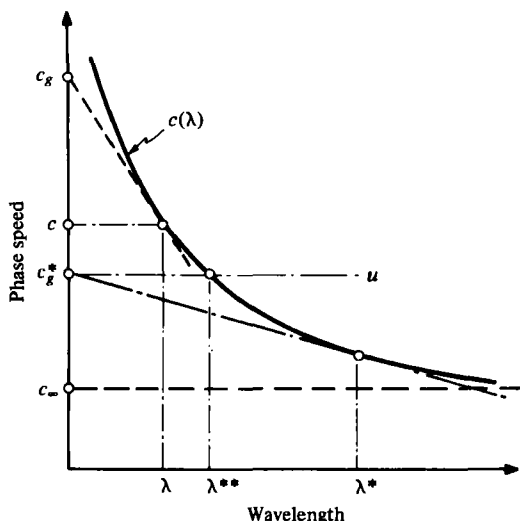
FIGURE 4. Dispersion relationship, $c(\lambda)$, according to equations (24) and (25).

(b) *The group velocity.* The energy in the dispersive wave system propagates at the group velocity, given by the expression (Whitham 1974)

$$c_g = c - \lambda \, dc/d\lambda = c[2 - (c_\infty/c)^2], \tag{25}$$

the last part of which is particular to the $c(\lambda)$ relationship of (24). Inspection of equation (24) shows that $dc/d\lambda < 0$, i.e. c increases monotonically as the wavelength shortens, hence

$$c_g(\lambda) > c(\lambda) > c_\infty \tag{26}$$

as in figure 4.

Consider now a *steady*, supercritical flow, such that $u > c_\infty$. If a particular source of disturbance, like a shock transition, produces wavelengths shorter than λ^*, for which $c_g^* = u$ (see figure 4), energy from the source in those wavelengths can radiate upstream. Furthermore, one particular wavelength, λ^{**}, will have an upstream phase speed exactly equal to the downstream flow velocity. That wavelength will therefore be perceived as a standing wave of area, as may be seen in part 1, figures 1, 10, 11 and 13.

By similar considerations, one may conclude that standing waves of area cannot appear *downstream* of a stationary area disturbance.

(c) *Relative importance of bending and tension.* Consider pure longitudinal bending waves (c_b), and pure tension waves (c_t), and introduce the relationships

$$K_p = [E(h/R_0)^3]/[12(1 - \nu^2)], \quad \nu = \tfrac{1}{2}, \quad \text{and} \quad T = \epsilon_x E h.$$

Then equation (24) yields

$$\frac{c_b}{c_t} \cong \frac{2(h/\lambda)}{\epsilon_x}.$$

In the experiments of part 1, h/λ ranged from 0·005 to 0·02, and ϵ_x from 0·023 to 0·174. Therefore $(c_b/c_t)^2$ was at most about 0·07. Considering the shortest waves ($\lambda \cong 5$ cm) and the smallest axial strain ($\epsilon_x = 0·023$), neglect of the last term in equation (24) would produce an error in c of only 8%.

Since this is so small, and in view of the approximate nature of the theory and the size of experimental error, longitudinal bending has been neglected in all that follows.
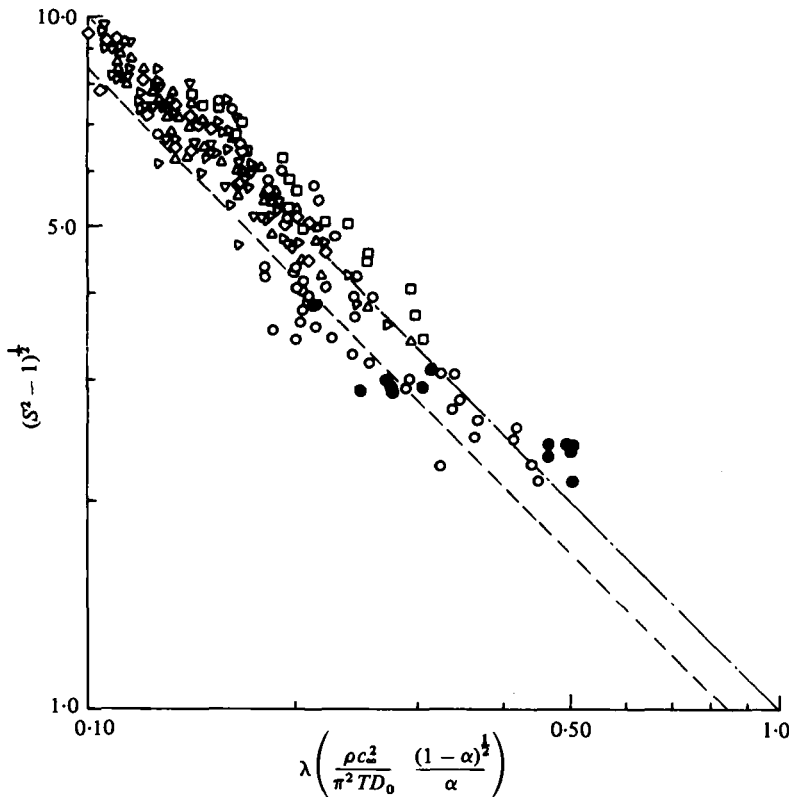
FIGURE 5. Comparison of measured and theoretical wavelengths. —·—, equation (27); ————, equation (27) reduced by 30% (see text); open symbols, steady flow experiments; closed symbols, unsteady flow experiments (Jan 1980). $\bigcirc$, $\epsilon_x = 0.023$; $\square$, 0.046; $\triangleright$, 0.091; $\triangle$, 0.110; $\triangledown$, 0.142; $\lozenge$, 0.174; $\bullet$, 0.016.

(d) *Comparison with experiments*. Returning to equation (23), and recalling that the coefficients of $(kD_0)^6$ and of (kD_0) are to be neglected, we calculate the wavelength of standing waves in a steady flow by setting $\bar{u} = c$. The result may be brought into the form

$$\lambda_0 \left(\frac{\rho c_\infty^2 (1-\bar{\alpha})^{\frac{1}{2}}}{\pi^2 T D_0 \bar{\alpha}} \right)^{\frac{1}{2}} = \frac{1}{(\bar{S}^2 - 1)^{\frac{1}{2}}}, \tag{27}$$

which is represented in figure 5 by the dot-dash line. If the formulation of the longitudinal stiffness is reduced by 30%, representing the outer limit of correction of (8) according to the calculations of Swidler (1980) for $\alpha \leqslant 0.8$, the theoretical relationship would be shown in figure 5 by the dashed line.

Using the area data for the tension–friction experiments of part 1, peak-to-peak and trough-to-trough wavelengths were measured, as well as the associated local mean values of $\bar{\alpha}$. For the other quantities appearing in (27), $c_\infty(\bar{\alpha})$ was determined from the local tube law (figure 7, part 1); $T = \epsilon_x Eh$ was determined from the measured strain ϵ_x and from a measured value of Eh ($= T/\epsilon_x$ in a calibrated stretching); and $\bar{S} = \bar{u}/c_\infty$, where $\bar{u} = Q/(A - A_p)$.

The experimental results for stationary waves are shown in figure 5 by the open

symbols. Except for a few points, largely those for low tension, all the data lie above the dashed line. These low points represent cases in which longitudinal bending may be of some significance: note that, for a given $\bar{S}$, (24) indicates a smaller theoretical wavelength if longitudinal bending is significant.

Considering the approximations of the theory and the magnitude of experimental error, the agreement between theory and experiment is most satisfactory, and lends credibility to the simple model representing the mechanics of the tube.

Also shown in figure 5 are the results of experiments in our laboratory on the refilling of a tube that over half of its length was initially in a state of partial collapse (Jan 1980). The main wave of refilling was preceded by propagating precursor waves due to tension. On the assumption that these were well dispersed, measurements of wavelength and speed of advance of the crests yielded the closed symbols of figure 5. Inasmuch as the apparatus was not long enough for the waves to be truly well dispersed, the agreement here is also quite satisfactory.

5. Wave growth in steady flow

From the preceding discussion, it appears that steady inviscid flow in a horizontal tube would exhibit standing waves of constant wavelength and amplitude, provided that a suitable source of disturbance were present. The experiments of part 1, however, show that the amplitude increases in the flow direction. That this is not primarily due to the increase in mean area associated with mean friction becomes evident from the gravity–friction experiments of part 1, in which the amplitude of area waves grows even though the equilibrium ratio, α_∞, remains constant.

This apparent downstream growth, it should be clear from §4, is in reality a manifestation in steady flow of the attenuation of waves radiated from the shock transition, which propagate upstream relative to the flow. In what follows, downstream 'growth' and upstream 'attenuation' signify the same phenomenon.

Here we consider only stationary waves in a steady flow. Accordingly we remove the time-dependence from (20) and (22) by setting $\omega = 0$. Furthermore, in (23) we set $c = 0$.

5.1. *Attenuation due to constant skin friction*

Equation (23) shows that, even with mean skin friction exactly balanced by gravity, the phase relationships in an area wave are such that mean skin friction affects the solution for $\alpha'(\xi)$. We may explore the influence of mean skin friction alone by setting $\hat{f} = 0$ in (23).

With these simplifications, (23) yields the following pair of simultaneous equations for k_r and k_i:

$$k_r^3 - 3k_r k_i^2 - \left[\frac{4\rho(\bar{u}^2 - c_\infty^2)}{TD_0\bar{\alpha}}\right]k_r = 0, \tag{28a}$$

$$k_i^3 - 3k_r^2 k_i + \left[\frac{4\rho(\bar{u}^2 - c_\infty^2)}{TD_0\bar{\alpha}}\right]k_i + \frac{24\rho\bar{u}^2\bar{f}}{TD_0^2\bar{\alpha}^2} = 0. \tag{28b}$$

Provided that $(k_i/k_0)^2 \ll 1/27$, where $k_0 = 2\pi/\lambda_0$ as given by (27) is the value of k_r for the inviscid case, the solution to (28) is approximated within $\pm 2\%$ by the expressions

$$k_i \simeq \frac{3\bar{f}}{D_0\bar{\alpha}}\left(\frac{\bar{S}^2}{\bar{S}^2 - 1}\right), \tag{29a}$$
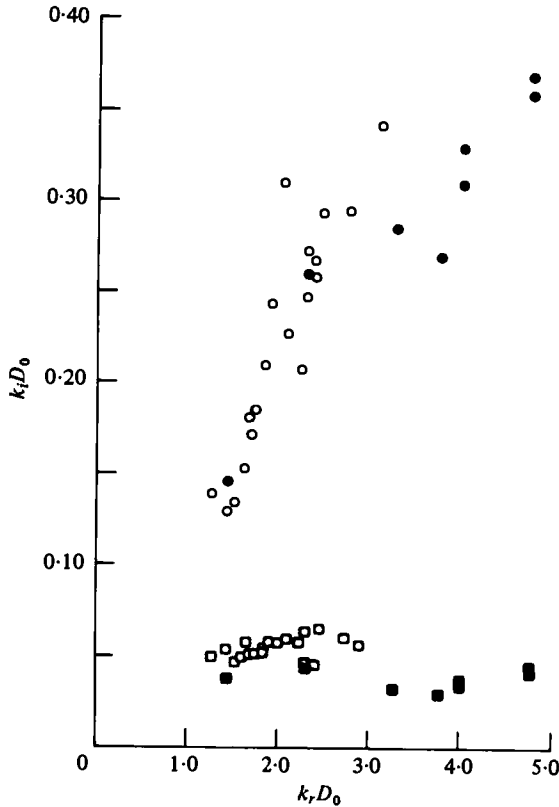
FIGURE 6. Growth coefficient *vs.* wavenumber. Open symbols, tension–friction flows; closed symbols, gravity–friction flows; circles, experimental data; squares, theoretical values based on mean skin friction coefficient, equation (29b).

$$k_r^2 = \left(\frac{2\pi}{\lambda}\right)^2 \simeq k_0^2[1 + 3(k_i/k_0)^2]. \tag{29b}$$

In the experiments of part 1, the ratio $k_0/k_i \sim 10$, hence the approximations above are reasonable. Equation (29b) shows that the wavelength is indeed affected only slightly by skin friction. However, as indicated by (29a), skin friction produces a streamwise growth (or upstream decay) of amplitude which is independent of both tension and wavelength. If $\bar{S} \gg 1$, the amplitude grows streamwise by the factor e in the distance $\Delta\xi = \bar{\alpha}/3\bar{f}$.

(a) *Comparison with experiments*. In the gravity–friction experiments, $\bar{\alpha} = \alpha_\infty$ was independent of ξ and the wave amplitudes were read directly off the strip chart showing $\alpha(\xi)$. In the tension–friction experiments, $\bar{\alpha}$ increased (almost linearly) with ξ; the wave amplitudes were interpreted as the oscillatory components superposed upon the mean curves of $\bar{\alpha}(\xi)$.

Graphs of log amplitude *vs.* ξ yielded reasonably straight lines, the slope of which was taken to be $k_i D_0$. Experimental values of $k_i D_0$ are shown in figure 6, plotted against the local wavenumber, $2\pi D_0/\lambda$. In each gravity–friction flow, λ was nearly constant, while in each tension–friction flow λ increased in the flow direction due to the frictional increase of $\bar{\alpha}$.

Figure 6 also compares the experimental data with theoretical values calculated from (29*a*); in the latter *f* was taken to be the value for turbulent flow represented by the upper lines in figures 2 and 3. Significant discrepancies are present between experiment and theory. Whereas the theory exhibits no effect of wavelength, the observed wave growth in fact increases substantially as the wavelength decreases. Moreover, the experimental growth rate is much larger than the theoretical, especially for short waves.

Clearly the observed growth rates cannot be explained by a mean skin-friction coefficient alone. Indeed, at large wavenumbers, the latter appears to play a small role if any.

5.2. *Wave growth due to curvature effects*

As the wavelength/diameter ratio decreases, several effects not hitherto considered come into play.

(i) Curvature of the streamlines, which is ignored in the one-dimensional theory, induces non-uniform velocity profiles. At an area minimum, for instance, the velocity near the wall tends to be larger than the average over the cross-section. For the same volume flow rate, the ratio of the actual momentum flux to the momentum flux carried by the one-dimensional mean velocity is always greater than unity, and increases with the degree of 'bowing' of the velocity profile. The streamwise gradient of this ratio (unaccounted for in the one-dimensional model) increases as the wavelength decreases.

(ii) Also associated with streamline curvature is a non-uniform pressure over the cross-section. At an area minimum, for instance, the pressure at the wall is lower than the average over the cross-section. In equation (5), the pressure loading on the wall, $p - p_e$, is determined by the wall pressure, whereas in equation (2) the pressure gradient $\partial p / \partial x$ relates to the average pressure over the cross-section. Consequently a discrepancy associated with wall curvature is present.

(iii) Because of the non-uniform velocity profile mentioned in (i), the effective velocity at the edge of the high shear layer near the wall is different from the one-dimensional mean velocity. At an area minimum, therefore, the shear stress tends to exceed that which would be associated with the mean velocity. In addition, the longitudinal pressure gradient, together with the time lags involving the adjustment of the boundary layer to the local longitudinal pressure gradient, produce effects on shear stress not accounted for in the one-dimensional theory.

A detailed analysis of the several phenomena listed above would be out of keeping with the nature of this paper. However, the several factors mentioned suggest a simple way of showing that even small wall curvature effects may cause large changes in wave growth. They also lead to a means for estimating how wavenumber affects growth rate.

Each of the three effects mentioned involves, in one way or another, a correction term to the momentum equation, (2). All three are associated with wavy-wall streamline curvature. In the context of the geometry of figure 1, we make the plausible conjecture that each correction term is represented principally by a quantity proportional to $d^2\alpha / d\xi^2$. We do not attempt here to deal with the three effects separately, nor do we deal specifically with the signs, phases and magnitudes of the respective proportionality constants. Instead, and with no purpose beyond showing the importance of such terms, we look at the effects of oscillatory skin friction alone.

(*a*) *Oscillatory skin friction.* Investigations of turbulent flow over a wavy plate

(Benjamin 1959; Zilker, Cook & Hanratty 1977) and of flow through a wavy pipe (Hsu 1968; Hsu & Kennedy 1971) show that the perturbation skin-friction coefficient f' (based on the *local* one-dimensional velocity) has a distinct sinusoidal form, both the amplitude and phase of which depend on the amplitude–wavelength ratio. For instance, in a pipe with a ratio of radius amplitude to wavelength of 1/45, the oscillatory amplitude of skin-friction coefficient is 48 % of the mean skin-friction coefficient, and the peak in f' is 26° upstream of the area minimum.

For the purpose of an illustrative calculation, we now suppose that f' peaks exactly at the area minimum, i.e. that it is 180° out of phase with the area oscillation. Thus we represent f' in equation (16c) by $r(d^2\alpha/d\xi^2)$, where r is a positive dimensionless constant. This is equivalent to expressing (22) as

$$f'(\xi) = r\hat{\alpha}(kD_0)^2 \exp[i(-kD_0\xi + \pi)]. \tag{30}$$

Then, setting $\hat{f} = r\hat{\alpha}(kD_0)^2$ and $\phi = \pi$, (23) is again solved for standing waves by setting $c = 0$. In the range where $(k_i/k_0)^2 \ll 1/27$, the results, accurate to $\pm 2\%$, are approximated by

$$k_i \simeq \frac{3\bar{f}}{D_0\bar{\alpha}}\frac{\bar{S}^2}{\bar{S}^2 - 1} + \frac{4\rho\bar{u}^2 r}{T}\frac{(1-\bar{\alpha})^{\frac{1}{2}}}{\bar{\alpha}}, \tag{31a}$$

$$k_r^2 = \left(\frac{2\pi}{\lambda}\right)^2 \simeq k_0^2 - k_i^2\left[1 - 4\frac{(k_i)_{r=0}}{k_i}\right]. \tag{31b}$$

As before, since $k_0/k_i \sim 10$, equation (31b) shows that friction has little effect on the wavelength.

Using equation (27) to eliminate T in equation (31a), we arrive at

$$k_i D_0 \simeq \frac{\bar{S}^2}{\bar{S}^2 - 1}\left[\frac{3\bar{f}}{\bar{\alpha}} + r(k_0 D_0)^2\right]. \tag{32}$$

Thus the oscillatory component of friction augments the growth rate $k_i D_0$ by an amount that is inversely proportional to the square of the wavelength. This is the same form of dependence associated with the attenuation of capillary waves on a free surface (Sorrell & Sturm 1977), although the mechanism of dissipation is different in its details.

(b) *An illustrative calculation.* In a typical experiment with an intermediate tension ($\epsilon_x = 0.11$), an intermediate speed index ($\bar{S} = 6.0$), and an area ratio $\bar{\alpha} = 0.40$, measurements of the area wave train gave the following values: $k_r = 2\pi/\lambda = 0.66$ cm^{-1}, $k_i = 0.076$ cm^{-1}, and $(d^2\alpha/d\xi^2)_{\text{peak}} = \pm 0.05$.

Using these values, and taking $\bar{f}$ from figure 3 as 0.0077, the value of the coefficient r required to satisfy (32) was found to be $r = 0.05$; correspondingly, $|f'|/\bar{f} = 0.3$. In this case, therefore, a properly phased, oscillatory skin-friction coefficient of modest amplitude (about one-third the mean skin-friction coefficient) increased the growth rate by threefold. There is too much scatter in the experimental data to ascertain how well the experimental data of figure 6 agree with the theoretical quadratic wave-number dependence shown in (32), but the general trend is correct.

The evidence seems quite convincing that effects lying outside the one-dimensional model account for a large part of the wave growth, particularly at the shorter wave-lengths.
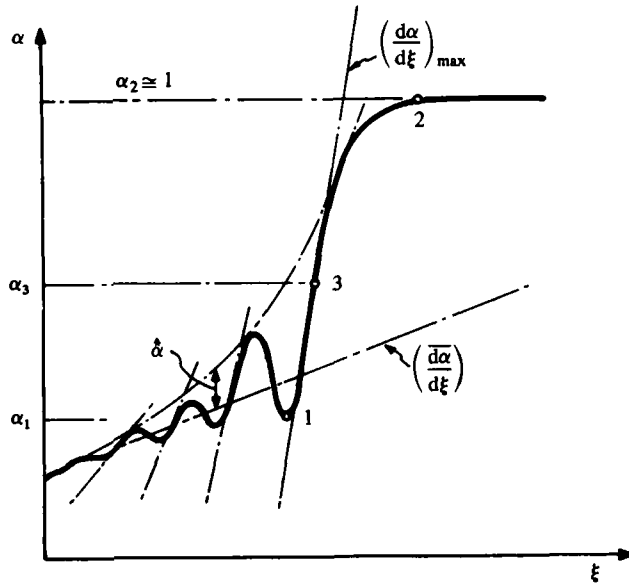
FIGURE 7. Schematic diagram of $\alpha(\xi)$.

6. Shock thickness

6.1. *Coupling of the wave train with the shock*

In part 1 data were presented for the static pressure recovery across a standing shock. Now we consider one detail of shock structure, namely the length of the shock, expressed in terms of the maximum slope $(d\alpha/d\xi)_{max}$ in the shock.

In figure 7, the shock is assumed to extend from point 1 to point 2, with point 3 lying at the position of maximum slope. Consider a reference frame in which the fluid upstream of the shock is stationary. The shock propagates toward the stationary fluid and also radiates disturbances, some of which, owing to the form of the dispersion relationship, race ahead of the shock in the form of area waves. Those area waves of length such that their phase speed matches the local mean fluid velocity stand stationary in the laboratory frame. Thought of in this way, the standing wave train in the steady flow and the standing shock wave which generates that train are inherently unseparable. The shock drives the wave train, and the segment 1–3 in figure 7 is both the front part of the shock and the rear of the wave train.

Although the wave amplitude in segment 1–3 is no longer small, we shall nevertheless attempt an estimate of the slope $(d\alpha/d\xi)_{max}$ at 3 by application of the linearized wave solution. For various reasons mentioned earlier, having to do both with the mechanics of the flow and the structural mechanics of the tube, the shape of the curve of $\alpha(\xi)$ in the final segment 3–2 of the shock lies outside the scope of this paper.

6.2. *Maximum slope of standing area waves*

The curve $\alpha(\xi)$ is expressed as the sum of two parts: one represents the virtually constant gradient due to a mean friction, the other represents the spatial area oscillations. Thus, utilizing equation (20) but with $\omega = 0$, we write

$$\alpha = \alpha_0 + \left(\frac{d\bar{\alpha}}{d\xi}\right)\xi + \hat{\alpha}\exp[-ik_r D_0\xi], \tag{33}$$

where $\hat{\hat{\alpha}} \equiv \hat{\alpha}\exp[k_i D_0\xi]$ represents the amplitude of the envelope (dashed in figure 7) of the area waves, taken with respect to the mean curve of constant slope $\overline{d\alpha/d\xi}$.

Differentiating (33), and using the maximum value of the slope $d\alpha/d\xi$, we form the parameter β, representing the ratio of the maximum oscillatory slope to the local wave amplitude:

$$\beta \equiv [(d\alpha/d\xi)_{\max} - (\overline{d\alpha/d\xi})]/\hat{\hat{\alpha}} = k_r D_0. \tag{34}$$

Ignoring the effects of friction on wavelength, we assume that $k_r = k_0$. Then, introducing $k_0 = 2\pi/\lambda_0$ from (27), and replacing T by $\epsilon_x Eh$, we get

$$\beta = \left[(\bar{S}^2 - 1)(1-\bar{\alpha})^{\frac{1}{4}}\left(\frac{\rho c_\infty^2}{E}\right)\left(\frac{D_0}{h}\right)\left(\frac{4}{\bar{\alpha}\epsilon_x}\right)\right]^{\frac{1}{4}}. \tag{35}$$

We note that $\overline{d\alpha/d\xi}$ is relatively small in (34); that, usually, the local value of $\bar{S} \gg 1$; and that, for a given tube, E, D_0 and h are constant, while c_∞ is nearly constant over a broad range of α. Accordingly, equation (35) shows that the inflection-point slope varies with the parameters of tension, speed index, and $\bar{\alpha}$ approximately in proportion to $(d\alpha/d\xi)_{\max} \sim \hat{\hat{\alpha}}\bar{S}(1-\bar{\alpha})^{\frac{1}{4}}/(\bar{\alpha}\epsilon_x)^{\frac{1}{4}}$.

6.3. *Steepness of shock*

(a) *Estimate based on wave train.* We now take the bold step of applying (35) to the segment 1–3 in order to estimate the maximum slope $(d\alpha/d\xi)$ of the shock. A few additional rough estimates are necessary, as follows: (i) the mean slope $\overline{d\alpha/d\xi}$ is ignored in comparison with $(d\alpha/d\xi)_{\max}$; (ii) we assume α_3 to lie midway between α_1 and α_2, and further assume that $\alpha_2 \simeq 1$, so that $\alpha_3 \simeq \frac{1}{2}(1+\alpha_1)$; (iii) we assume the amplitude $\hat{\hat{\alpha}}_3$ at the shock to be half the final jump in α, that is, $\hat{\hat{\alpha}}_3 = \frac{1}{2}(\alpha_2 - \alpha_1) = \frac{1}{2}(1-\alpha_1)$; (iv) the speed index S_3 is assumed sufficiently large so that $(S_3^2 - 1) \simeq S_3^2$; (v) the wave speed c_∞ is taken to be constant over the range 1–3.

With these assumptions, and with the help of the continuity equation to relate states 1 and 3, namely $u_3\alpha_3 = u_1\alpha_1$, equation (35) applied to the wave segment 1–3 yields

$$\left(\frac{d\alpha}{d\xi}\right)_3 \simeq \frac{S_1}{\epsilon_x^{\frac{1}{2}}}\frac{\alpha_1(1-\alpha_1)^{\frac{1}{4}}}{(1+\alpha_1)^{\frac{3}{4}}}\left(\frac{8}{\sqrt{2}}\frac{\rho c_\infty^2}{E}\frac{D_0}{h}\right)^{\frac{1}{4}}. \tag{36}$$

(b) *Physical consideration of shock steepness.* A result similar to (36) may be obtained which does not depend on the wave train calculation, but rather proceeds from physical arguments, as follows.

The deceleration through a stationary shock, $u\,\partial u/\partial x$, entails a pressure rise which accounts for the area increase to the inflated condition, $\alpha \simeq 1$.

Due to nonlinearities, a propagating shock of large amplitude tends to steepen. Its stationary form is ultimately determined by a balance between two competitive effects:

(i) the steepening effects of inertia, and (ii) the mechanical stiffness against steepening due to longitudinal tension and bending. For the present argument we consider only tension; bending would act somewhat similarly.

In order to make an order-of-magnitude estimate of the stationary shock form, we assume that in (2) the two terms $u\,du/dx$ and $(1/\rho)\,\partial p/\partial x$ are dominant. Thus they must be of the same order of magnitude. However, if the tendency of the pressure rise to open the tube rapidly is resisted mainly by longitudinal tension, then the 'inertial pressure', $\frac{1}{2}\rho u_1^2$, must be of the same order of magnitude as the 'tension pressure', ΔP_t. Using equation (8), we write

$$\frac{\rho u_1^2}{2} \simeq \frac{T/D_0}{4(1-\alpha)^{\frac{3}{2}}}\frac{d^2\alpha}{d\xi^2}. \tag{37}$$

When this is combined with assumptions like those that led to (36), we get a result of exactly the same form, but with greater uncertainty as to the magnitude of the numerical coefficient.

The physical arguments outlined here suggest, however, that (36) overestimates the shock steepness because it neglects the unsteepening effect of longitudinal bending, an effect which may be important in shocks.

6.4. *Comparison with experiments*

The maximum shock gradients $(d\alpha/d\xi)_s$, as determined graphically from the data of the tension–friction experiments of part 1, are plotted in figure 8. Also shown as a straight line is the theoretical estimate of (36).

The data exhibit considerable scatter, owing to the difficulty of measuring $(d\alpha/d\xi)_s$. However, both in form and scale, the results are in general agreement with the model here suggested, confirming that the forward part of the shock and the rearward part of the wave train are indeed the same.

The lower points in figure 8 are associated with the smallest axial tensions. In those cases longitudinal bending would be relatively more important as a stiffness against shock steepening, and would tend to decrease the shock slope, in agreement with the data.

7. Numerical experiments

In this section results are presented based on numerical integrations which take account of nonlinearities in the governing equations. We consider steady, initially supercritical flows in a horizontal tube, with significant longitudinal tension and friction, but negligible longitudinal bending.

The general objectives of the numerical experiments were to explore the limits of the linearized theory and to obtain some insight into nonlinear effects associated with large amplitudes.

7.1. *The calculational model*

(a) *Tube law.* In §2 it was pointed out that the structural model on which (7) is based is not valid as $\alpha \to 1$, and that this is in part reflected by the blow-up of the term $(1-\alpha)^{\frac{1}{2}}$ in the denominator. Since this term is not in any case strongly nonlinear, except as $\alpha \to 1$, it has been set equal to unity for the numerical experiments.

We also neglect the nonlinear term in $(d\alpha/d\xi)^2$ in (7), partly because it is usually
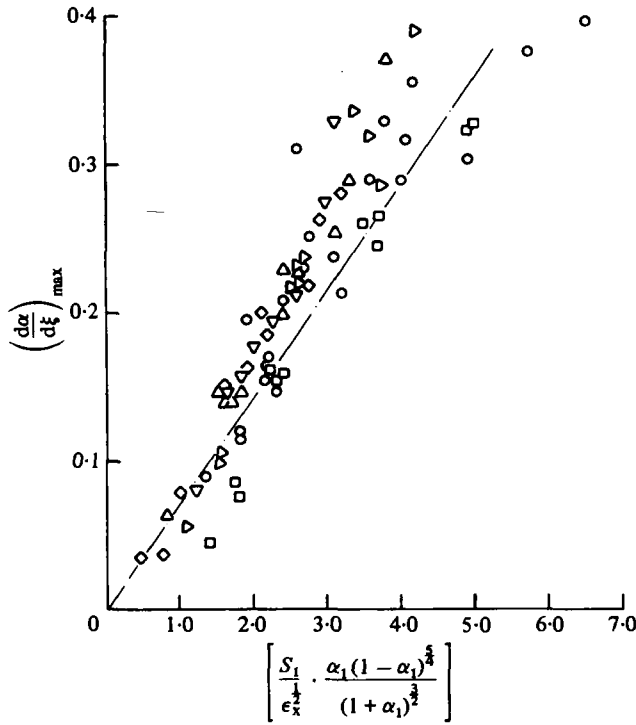
FIGURE 8. Shock steepness. Open points, experimental data (symbols correspond to figure 5); —, equation (36).

small compared with the leading linear term, and partly because its nonlinear influence is small compared with the strong nonlinearity due to the term α^{-3} that appears subsequently.

The several assumptions above, applied to (5) and (7), lead to the expression

$$p - p_e = K_p \mathscr{P}(\alpha) - \frac{T}{4D_0} \frac{d^2\alpha}{d\xi^2}. \tag{38}$$

(b) *The governing equation.* Assuming T and p_e both constant, dp/dx is calculated from (38) and substituted into (2), with the further simplifications that $\partial/\partial t = 0$, $\partial/\partial \xi = d/d\xi = 0$. The result is combined with (1) in the form $d(uA)/d\xi = 0$. Finally one obtains

$$\frac{d^3\alpha}{d\xi^3} = \frac{4\rho u_0^2 D_0}{T\alpha^3} \left[\frac{1 - S^2}{S^2} \frac{d\alpha}{d\xi} + 2f \right], \tag{39}$$

in which the nonlinearities are the strong one in α^{-3} and the weak one in $(1 - S^2)/S^2$.

The tension term, $T d^3\alpha/d\xi^3$, in (39) radically changes the possible behaviour patterns. In the absence of tension, the term $1 - S^2$ changes the sign of $d\alpha/d\xi$ at $S = 1$. Consequently the integral curves admit the possibilities of (i) choking when $S = 1$; and (ii) continuous transitions between $S < 1$ and $S > 1$, but only on singular curves (Shapiro 1977). With tension present, on the other hand, the character of the governing equation changes, and the aforenamed possibilities, familiar from gasdynamics and free-surface flows, disappear.
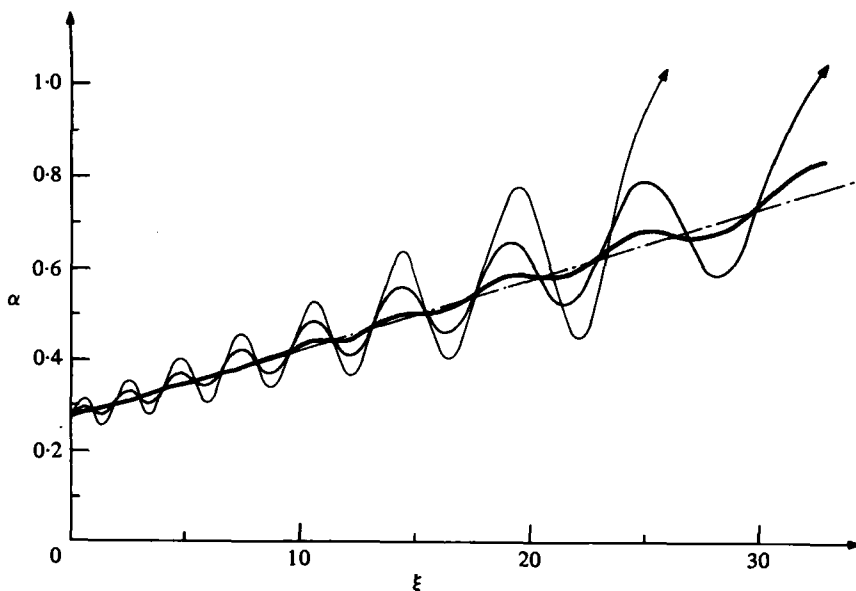
FIGURE 9. Numerical integrations, with $S_0 = 10 \cdot 0$, $\alpha_0 = 0 \cdot 275$, $\epsilon_x = 0 \cdot 10$, $f = 0 \cdot 007\,42$.
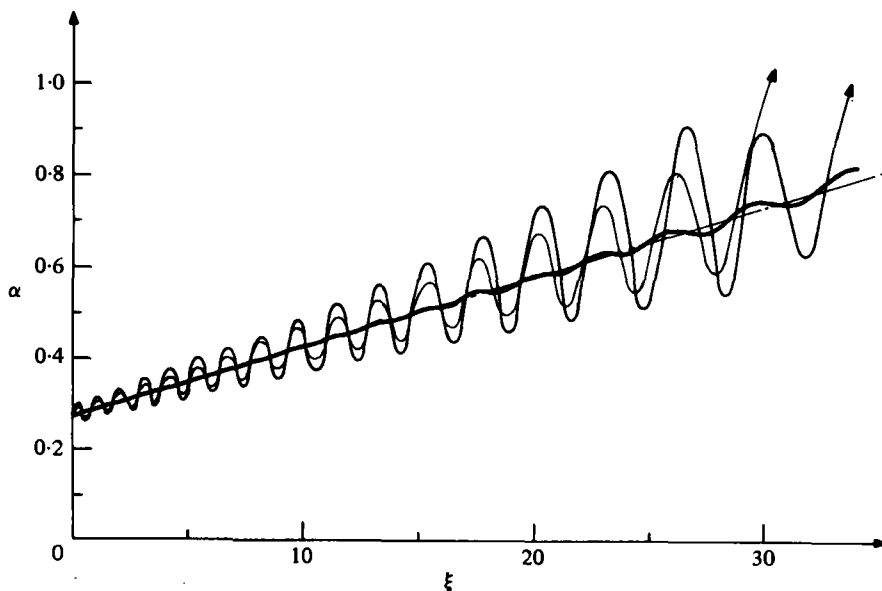
FIGURE 10. Numerical integrations, with $S_0 = 10 \cdot 0$, $\alpha_0 = 0 \cdot 275$, $\epsilon_x = 0 \cdot 025$, $f = 0 \cdot 007\,35$. Heavy line, $(d\alpha/d\xi)_0 = 0 \cdot 30$; medium line, $(d\alpha/d\xi)_0 = 0 \cdot 135$; light line, $(d\alpha/d\xi)_0 = 0 \cdot 195$.

(c) *Numerical procedure.* Three boundary conditions on α and its derivatives are needed in order to obtain solutions to (39). In the physical experiments, the latex tube is compressed by the sphincter at the upstream end and is attached to a rigid tube at the downstream end; thus α is physically established at the two ends. A third boundary condition, on the values of α and $d^2\alpha/d\xi^2$ at the downstream end, is determined physically by the level of downstream pressure. Since the flow rate Q (to which both u_0 and S are related) is constant, $dQ/d\xi = 0$. Use of this converts (39) into a differential
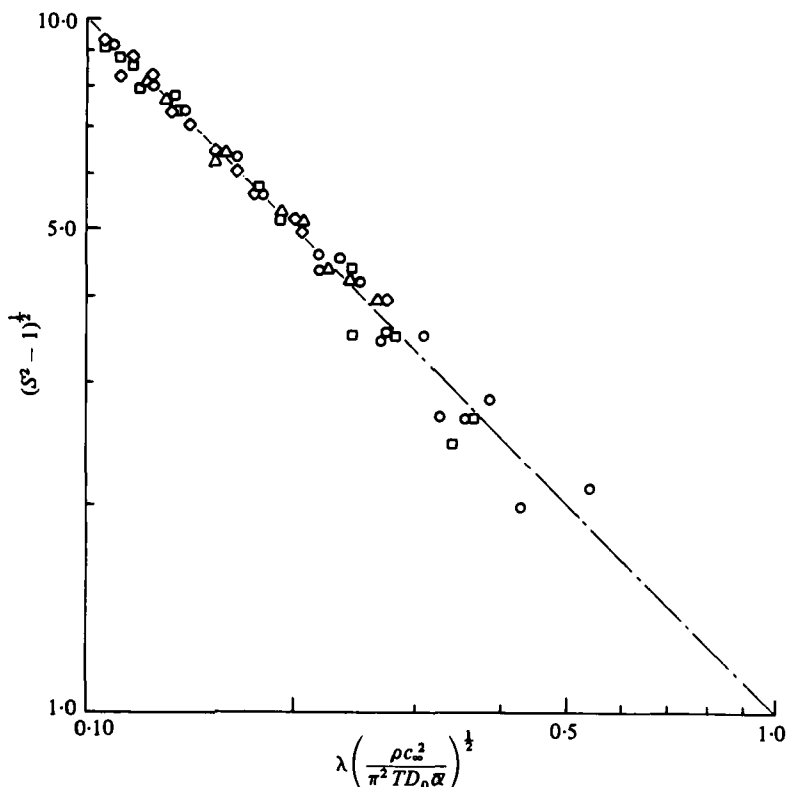
FIGURE 11. Comparison of wavelengths from numerical integrations (points) with line representing equation (27), from which the factor $(1-\alpha)^{\frac{1}{2}}$ has been deleted. $\bigcirc$, $\epsilon_x = 0.025$; $\square$, 0.050; $\diamondsuit$, 0.100; $\triangle$, 0.200.

equation of fourth order. The fourth boundary condition that then becomes necessary is provided physically by the inlet pressure, which is connected to the values of α and $d^2\alpha/d\xi^2$ at the inlet end.

These boundary conditions are mathematically of jury type. Brower (1970) attempted numerical integrations of flows with subcritical inlet states, using such boundary conditions. Not surprisingly, a cumbersome and time-consuming iterative technique was required to match the physical boundary conditions. Furthermore, the adjustment of the area to the downstream rigid area often occurs in a relatively short distance, and it would be inappropriate to neglect longitudinal bending moments in such an end region.

For the numerical experiments, therefore, we did not attempt to simulate the physical experiments in entirety but rather we set out to explore numerically certain phenomena. Accordingly, equation (39) was integrated not with the physical boundary conditions but rather with alternate conditions for which the problem was of marching type. Values of α_0, $(d\alpha/d\xi)_0$ and $(d^2\alpha/d\xi^2)_0$ were selected at one location, together with a value for Q, and the equation was then integrated forwards in ξ. The value of α_0 was chosen arbitrarily; $(d^2\alpha/d\xi^2)_0$ was set equal to zero; and $(d\alpha/d\xi)_0$ was given various arbitrary values. The difference between the chosen value of $(d\alpha/d\xi)_0$ and the value of the friction-induced mean gradient $\overline{d\alpha/d\xi}$ for the tension-free case represented an input
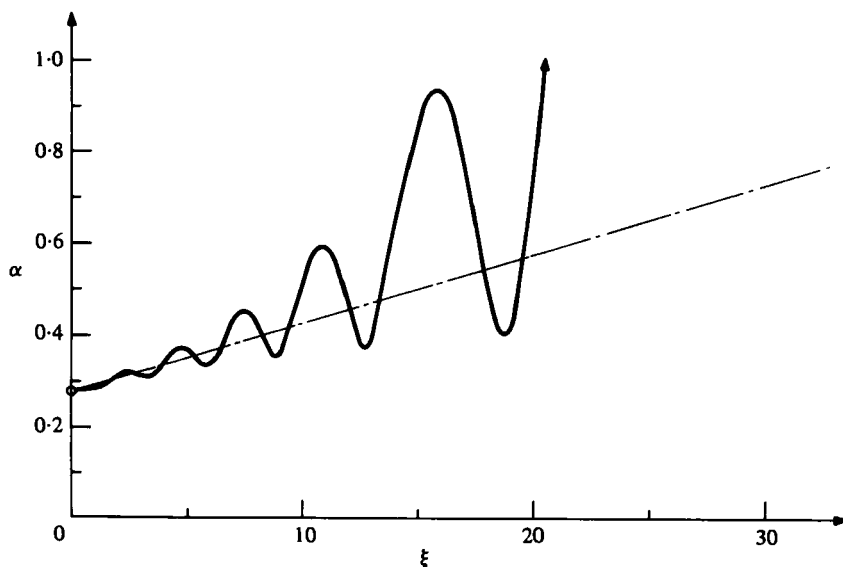
FIGURE 12. Numerical integration. Same conditions as for figure 9, but with oscillatory skin-friction coefficient ($r = 0.03$), and with $(d\alpha/d\xi)_0 = 0.03$. Dot-dash line is initial mean slope $\overline{d\alpha/d\xi}$.

disturbance which generated tension waves; the larger this difference, the larger the computed wave amplitude.

In carrying out this procedure, (39) was reduced to a system of three simultaneous first-order, ordinary nonlinear differential equations. A standard fourth-order Runge–Kutta routine was then used to integrate the system of equations numerically (Hornbeck 1975). A spatial step size of magnitude $\Delta\xi = 1/40$ gave satisfactory results with respect to stability and truncation error.

7.2. *Results of forward integrations*

(a) *Constant skin-friction coefficient.* Figure 9 shows computed results for a case with moderately large tension and with three different amplitudes of input disturbance. Figure 10 refers to the same initial values of α_0 and S_0, but with a tension one-fourth as large. The numerical results show the same general behaviour as the experiments (part 1). Superposed upon a mean (and nearly linear) gradient $\overline{d\alpha/d\xi}$ due to friction is a standing wave whose amplitude increases in the downstream direction.

As one expects intuitively, and in agreement with the experimental data (part 1) and the linearized theory, tension increases the wavelength. For small amplitudes, the wavelength is independent of amplitude. As the amplitude gets large, however, the wavelength increases.

From integrations like those of figures 9 and 10, peak-to-peak and trough-to-trough wavelengths were measured for cases with amplitudes of α of the order of 0·1. In figure 11 these are compared with the theoretical, small-amplitude, inviscid dispersion relationship of (27), but with the factor $(1 - \bar{\alpha})^{\frac{1}{2}}$ omitted since it was omitted in (38) and (39). The scatter of the points about the small-amplitude theoretical line arises from two sources. One is the error in λ due to purely numerical truncation errors in the integrations. The other is that (27) applies to precisely sinusoidal waves in a flow
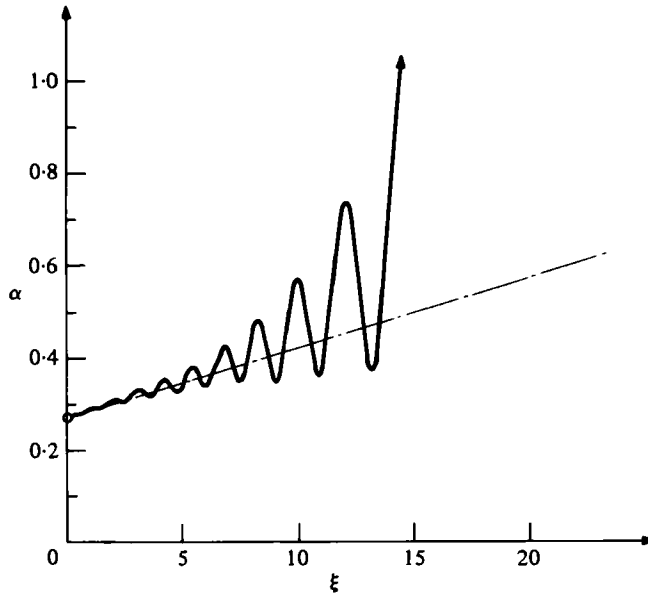
FIGURE 13. Numerical integration. Same conditions as for figure 10, with oscillatory skin-friction coefficient $(r = 0.01)$, and with $(d\alpha/d\xi)_0 = 0.03$. Dot-dash line is initial mean slope $\overline{d\alpha/d\xi}$.

without friction and with no mean gradient in α; apart from the effect of friction on the phase speed, errors are introduced because one has to select, from outputs like those of figures 9 and 11, the mean values of S and $\bar\alpha$ appropriate to a particular wave of length λ.

The significant conclusion to be reached from figure 11, therefore, is that the inviscid dispersion relationship is generally accurate even with non-sinusoidal, growing waves in a frictional flow which has a mean gradient $\overline{d\alpha/d\xi}$.

Growth rates (or decay rates in the $-\xi$ direction) for the wave trains shown in figures 9 and 10 compare well with the small-amplitude theoretical result of (29a). For very small amplitude waves the comparison is within $\pm 2\%$. When the amplitude $\hat{\alpha}$ becomes quite large, say $\hat{\alpha} > 0.10$, the linearized result begins to fail. Furthermore, as S approaches unity in some part of the wave, (29a) shows extremely rapid wave growth, which concomitantly induces large amplitudes that vitiate the linearized results. This behaviour suggests that the amplifying oscillatory wave terminates itself as a shock when the area grows so large that the tube becomes much stiffer and the flow becomes subcritical.

(b) *Oscillatory skin-friction coefficient.* Figures 12 and 13 correspond to figures 9 and 10, respectively, but they show the effects of an oscillatory component of skin-friction coefficient $f' = r\,d^2\alpha/d\xi^2$.

A comparison of figure 12 with 9, and of figure 13 with 10, shows that a small component f' greatly increases the growth rate of the waves, and also causes the waves to become more asymmetrical. Furthermore, the mean slope $\overline{d\alpha/d\xi}$ is not constant, but increases progressively as the amplitude grows.

The growth rates about the mean gradient line were compared with values calculated from (32). For the first three or four waves, when the peaks and troughs are still reason-

ably symmetric about the mean gradient line, the peaks decay at a rate about 10 % larger than the linearized results, while the troughs decay at a rate about 10 % less. Similar numerical integrations for cases in which there is no mean gradient and the amplitudes are very small yield results in agreement with (32).

REFERENCES

BENJAMIN, K. B. 1959 Shearing flow over a wavy boundary. *J. Fluid Mech.* 6, 161–205.

BROWER, R. W. 1970 Pressure–flow characteristics of collapsible tubes. Ph.D. thesis, University of Pennsylvania.

FLAHERTY, J. E., KELLER, J. B. & RUBINOW, S. I. 1972 Post-buckling behaviour of elastic tubes and rings with opposite sides in contact. *SIAM J. Appl. Math.* 23, 446–455.

HORNBECK, R. W. 1975 *Numerical Methods*, p. 195. New York: Quantum.

HSU, S. 1968 Turbulent flow in wavy pipes. Ph.D. thesis, University of Iowa.

HSU, S. & KENNEDY, J. F. 1971 Turbulent flow in wavy pipes. *J. Fluid Mech.* 47, 481–502.

JAN, D. L. 1980 Refilling of collapsible tubes. M.S. thesis, Massachusetts Institute of Technology.

KECECIOGLU, I. 1979 Experimental determination of the structure of shock waves in fluid flow through collapsible tubes with application to the design of a flow regulator. Thesis for the Degree of Mechanical Engineer, Massachusetts Institute of Technology.

KECECIOGLU, I., McCLURKEN, M. E., KAMM, R. D. & SHAPIRO, A. H. 1981 Steady, supercritical flow in collapsible tubes. Part 1. Experimental observations. *J. Fluid Mech.* 109, 367–389.

McCLURKEN, M. E. 1980 Supercritical flow in collapsible tubes. Ph.D. thesis, Department of Mechanical Engineering, Massachusetts Institute of Technology.

SCHLICHTING, H. 1968 *Boundary Layer Theory*, 6th edn. McGraw-Hill.

SHAPIRO, A. H. 1977 Steady flow in collapsible tubes. *Trans. A.S.M.E., J. Biomech. Engng* 99, 126–147.

SORRELL, F. Y. & STURM, G. V. 1977 The interaction between capillary waves and a current and wave decay. *J. Fluid Mech.* 81, 241–256.

SWIDLER, S. C. 1980 Effect of longitudinal tension and curvature on pressure–area relationships of collapsible tubes. M.S. thesis, Dept. of Mechanical Eng., Massachusetts Institute of Technology.

WHITHAM, G. B. 1974 *Linear and Nonlinear Waves.* Wiley.

ZILKER, D. P. COOK, G. W. & HANRATTY, T. J. 1977 Influence of the amplitude of a solid wavy wall on a turbulent flow. Part 1. Non-separated flows. *J. Fluid Mech.* 82, 29–51.